Journal of Rock Mechanics and Geotechnical Engineering. 2011, 3 (3): 193–206

Journal of Rock Mechanics and Geotechnical Engineering

Journal online: www.rockgeotech.org

A generalized multi-field coupling approach and its application to stability and deformation control of a high slope

Chuangbing Zhou[1, 2*], Yifeng Chen[1, 2], Qinghui Jiang[1, 2], Wenbo Lu[1, 2]

[1] *State Key Laboratory of Water Resources and Hydropower Engineering Science, Wuhan University, Wuhan, 430072, China*

[2] *Key Laboratory of Rock Mechanics in Hydraulic Structural Engineering of Ministry of Education, Wuhan University, Wuhan, 430072, China*

Received 14 April 2011; received in revised form 15 July 2011; accepted 28 July 2011

Abstract: Human activities, such as blasting excavation, bolting, grouting and impounding of reservoirs, will lead to disturbances to rock masses and variations in their structural features and material properties. These engineering disturbances are important factors that would alter the natural evolutionary processes or change the multi-field interactions in the rock masses from their initial equilibrium states. The concept of generalized multi-field couplings was proposed by placing particular emphasis on the role of engineering disturbances in traditional multi-field couplings in rock masses. A mathematical model was then developed, in which the effects of engineering disturbances on the coupling-processes were described with changes in boundary conditions and evolutions in thermo-hydro-mechanical (THM) properties of the rocks. A parameter, ***d***, which is similar to damage variables but has a broader physical meaning, was conceptually introduced to represent the degree of engineering disturbances and the couplings among the material properties. The effects of blasting excavation, bolting and grouting in rock engineering were illustrated with various field observations or theoretical results, on which the degree of disturbances and the variations in elastic moduli and permeabilities were particularly focused. The influences of excavation and groundwater drainage on the seepage flow and stability of the slopes were demonstrated with numerical simulations. The proposed approach was further employed to investigate the coupled hydro-mechanical responses of a high rock slope to excavation, bolting and impounding of the reservoir in the dam left abutment of Jinping I hydropower station. The impacts of engineering disturbances on the deformation and stability of the slope during construction and operation were demonstrated.

Key words: generalized multi-field couplings; engineering disturbance; slope stability; deformation control

1 Introduction

In the last three decades, there has been an increasing interest in the multi-field couplings within rock masses due to the requirements of performance assessment and optimization design in radioactive waste disposal, geothermal energy utilization, deep mining, etc. The term "multi-field coupling" implies that one process, for example, the fluid flow, affects the initiation and progress of another (e.g. the stress-strain process) [1]. Even in dam engineering or rock slope engineering, the deformation and stability of a dam foundation or rock slope, which are the major concerns in design, cannot be fully understood when only the stress-strain process is considered.

In rock mechanics, the concept of multi-field couplings is basically used to represent the interactions among stress, seepage and thermal fields. These coupled processes are actually involved in the formation and evolution processes of rock masses. Excavation and other human activities lead to disturbances to the near-field of the rock masses, causing variations in their structural features and thermo-hydro-mechanical (THM) properties. For rock slopes in hydropower engineering, the sources of engineering disturbances may include blasting excavation, bolt reinforcement, consolidation grouting, groundwater drainage, concrete replacement, fluctuation of reservoir water level, etc.

The formation and evolution of a rock mass are

Doi: 10.3724/SP.J.1235.2011.00193

*Corresponding author. Tel:+86-27-68774295; E-mail: cbzhou@whu.edu.cn

Supported by the National Natural Science Fund for Distinguished Young Scholars of China (50725931), the National Natural Science Foundation of China (50839004, 51079107) and the Supporting Program of the "Eleventh Five-year Plan" for Sci & Tech Research of China (2008BAB29B01)

inherent natural processes affected by various internal and external geological agents, and by engineering disturbances induced by human activities. In a common sense, the engineering disturbances can also be considered as a process that triggers or strengthens the existing natural multi-field couplings in the rock masses [2, 3]. Compared to the natural evolutionary processes, this man-made process is more controllable because each source of disturbances can be well designed and adjusted as needed, by taking into account the geological features of the rock masses concerned, the stability requirements of the projects, and the allowable deformation of the engineered rock masses. Therefore, the natural multi-field coupling processes and the engineering disturbances can form a generalized multi-field coupling system.

In this study, a concept of generalized multi-field couplings is proposed for engineered rock masses, on which the effects of engineering disturbances on the natural coupling processes are particularly concentrated [2, 3]. Theoretically, a generalized multi-field coupling model has the same form as the traditional multi-field coupling models [4, 5], but more emphases are placed on the effects of engineering disturbances, engineered rock utilization and alteration, and the process control of rock deformation and stability. As a result, the deformation and failure mechanisms and the evolution of rock stability can be better understood.

The stability analysis and deformation control of rock slopes in hydropower engineering are reported in terms of generalized multi-field couplings. Major concerns are placed on the mathematical model for generalized multi-field couplings and the effects of engineering disturbances and seepage flow on slope stability.

2 A generalized multi-field coupling approach

Mathematically, the presence of engineering disturbances will change the boundary conditions and the properties of an engineered rock mass, and thus the coupled THM processes in rock masses may be altered, as shown in Fig.1. The generalized coupling processes in a rock mass are basically governed by the same conservation equations as the traditional coupled THM processes for geological media and systems. However, more emphases need to be placed on the boundary conditions and material properties, since the disturbances most likely play a more important role in their alteration and/or evolution.

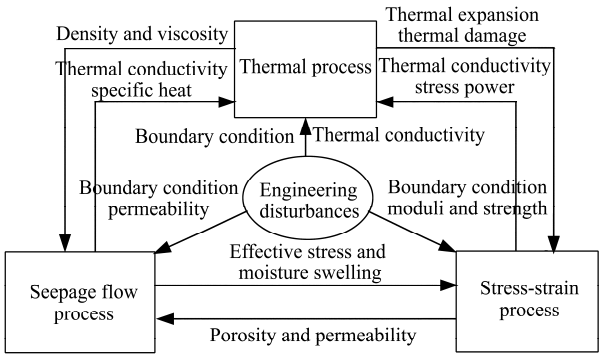

Fig.1 Generalized multi-field coupling processes in rock masses.

To derive the governing equations, the following assumptions are considered:

(1) A representative elementary volume (REV) exists for the concerned rock mass so that the problem can be addressed in the framework of continuum mechanics.

(2) The assumptions of small deformation and quasi-static state are made for mechanical responses, and the modified Terzaghi's effective stress principle is assumed for both saturated and unsaturated states [6].

(3) Gas pressure in the voids is assumed to be constant (equal to the atmosphere pressure p_a) in the unsaturated state, where water phase exchange and steam production in the voids are the minor concerns.

(4) Fluid movement follows the generalized Darcy's law, and heat conduction is governed by the generalized Fourier's law.

With the above assumptions, the governing equations for the coupled THM processes [6] are given by:

(1) Equations of conservation of momentum

The equations of conservation of momentum can be written as

$$\nabla\cdot\left[\boldsymbol{D}:\nabla\left(\frac{\partial \boldsymbol{u}}{\partial t}\right)-\alpha\frac{\partial p}{\partial t}\boldsymbol{\delta}\right]+\frac{\partial \rho}{\partial t}\boldsymbol{g}=0 \tag{1}$$

where t is the time, $\boldsymbol{D}$ is the fourth-order tangential elastic modulus tensor of the medium, $\boldsymbol{u}$ is the displacement vector, ρ is the density, p is the pore water pressure, α is the effective stress parameter, and $\boldsymbol{g}$ is the gravitational acceleration vector.

In a saturated condition, α can be represented as $\alpha = 1 - K/K_s$, where K and K_s are the drained bulk moduli of medium and solid grains, respectively.

(2) Equation of mass conservation of seepage flow

The equation of mass conservation of seepage flow

can be written as

$$\nabla\cdot\left[\rho_{\mathrm{w}}\frac{k_{\mathrm{r}}\boldsymbol{k}}{\mu}(\nabla p-\rho_{\mathrm{w}}\boldsymbol{g})\right]=\rho_{\mathrm{w}}nS_{\mathrm{r}}\frac{\partial\varepsilon_{\mathrm{v}}}{\partial t}+$$

$$\rho_{\mathrm{w}}n(S_{\mathrm{r}}c_{\mathrm{w}}-c_{\mathrm{S}})\frac{\partial p}{\partial t}+\rho_{\mathrm{w}}S_{\mathrm{r}}\frac{\partial n}{\partial t} \tag{2}$$

where $\boldsymbol{k}$ is the intrinsic permeability tensor of the medium; k_{r} is the relative permeability of water; ρ_{w} is the density of water; μ is the dynamic viscosity of water; n is the porosity; ε_{v} is the volumetric strain; S_{r} is the degree of saturation; c_{w} is the coefficient of compressibility of water; and c_{S} is defined as $c_{\mathrm{S}}=\partial S_{\mathrm{r}}/\partial s$, where $s=p_{\mathrm{g}}-p$ is the matrix suction.

(3) Equation of conservation of energy

The equation of conservation of energy can be considered as

$$\nabla\cdot\left[\boldsymbol{\sigma}\frac{\partial\boldsymbol{u}}{\partial t}+p\frac{k_{\mathrm{r}}\boldsymbol{k}}{\mu}(\nabla p-\rho_{\mathrm{w}}\boldsymbol{g})+\boldsymbol{\lambda}\nabla T\right]=$$

$$[(1-n)\rho_{\mathrm{s}}C_{\mathrm{s}}+nS_{\mathrm{r}}\rho_{\mathrm{w}}C_{\mathrm{w}}+n(1-S_{\mathrm{r}})\rho_{\mathrm{g}}C_{\mathrm{g}}]\frac{\partial T}{\partial t}-\rho\boldsymbol{g}\frac{\partial\boldsymbol{u}}{\partial t}-$$

$$\left(1-\frac{c_{\mathrm{S}}}{S_{\mathrm{r}}}p\right)\boldsymbol{v}\nabla p_{\mathrm{w}}+\rho_{\mathrm{w}}C_{\mathrm{w}}\boldsymbol{v}\nabla T \tag{3}$$

where T is the temperature; $\boldsymbol{\sigma}$ is the stress tensor; ρ_{s} and ρ_{g} are the densities of solid grains and gas, respectively; C_{s}, C_{w} and C_{g} are the specific heat capacities of solid grains, water and gas, respectively; $\boldsymbol{\lambda}$ is the thermal conductivity tensor of the medium; and $\boldsymbol{v}$ is the Darcy's velocity of water.

In the coupled system, the porosity n evolves in the following manner [6]:

$$n=\alpha-(\alpha-n_0)\exp\left(-\varepsilon_{\mathrm{v}}-\frac{\alpha}{K_{\mathrm{s}}}\Delta p\right) \tag{4}$$

where n_0 is the initial porosity.

If the solid grains are assumed to be incompressible, Eq.(4) can be reduced to

$$n=1-(1-n_0)\exp(-\varepsilon_{\mathrm{v}}) \tag{5}$$

The governing equations, Eqs.(1)–(3), are subjected to the following initial conditions:

$$\left.\begin{aligned}&\boldsymbol{u}(0)=\boldsymbol{u}_0\\&p(0)=p_0\\&T(0)=T_0\end{aligned}\right\}\quad(\text{in }\Omega) \tag{6}$$

where $\boldsymbol{u}_0$, p_0 and T_0 are the initial displacement vector, water pressure and temperature, respectively.

The following boundary conditions should also be satisfied:

$$\boldsymbol{u}=\hat{\boldsymbol{u}}\ (\text{on }\Gamma_u),\ p=\hat{p}\ (\text{on }\Gamma_{\mathrm{w}}),\ T=\hat{T}\ (\text{on }\Gamma_{\mathrm{T}}) \tag{7}$$

$$\left.\begin{aligned}&\boldsymbol{t}\equiv\boldsymbol{\sigma}\boldsymbol{n}=\hat{\boldsymbol{t}} && (\text{on }\Gamma_\sigma)\\&q_{\mathrm{w}}\equiv-\rho_{\mathrm{w}}\boldsymbol{v}\boldsymbol{n}=\hat{q}_{\mathrm{w}} && (\text{on }\Gamma_{\mathrm{w}}^{q})\\&q_{\mathrm{T}}\equiv-\boldsymbol{i}\boldsymbol{n}=\hat{q}_{\mathrm{T}} && (\text{on }\Gamma_{\mathrm{T}}^{q})\end{aligned}\right\} \tag{8}$$

where Γ_u and Γ_σ are the displacement and traction boundaries, respectively; Γ_{w} and Γ_{w}^{q} are the water pressure and flux boundaries, respectively; Γ_{T} and Γ_{T}^{q} are the thermal boundaries with given temperature and flux, respectively; $\hat{\boldsymbol{u}}$ and $\hat{\boldsymbol{t}}$ are the given displacement and traction vectors on the boundaries, respectively; $\hat{p}$ and $\hat{q}_{\mathrm{w}}$ are the given water pressure and flux, respectively; $\hat{T}$ and $\hat{q}_{\mathrm{T}}$ are the given temperature and thermal flux, respectively; $\boldsymbol{i}$ is the heat conduction flux vector; and $\boldsymbol{n}$ is the outward unit normal vector on the boundaries.

A generalized multi-field coupling model emphasizes the effects of engineering disturbances on the coupled THM processes through the boundary conditions, Eqs.(7) and (8), and the constitutive relations and material properties (i.e. $\boldsymbol{D}$, $\boldsymbol{k}$ and $\boldsymbol{\lambda}$). The drilling and blasting excavation, for example, presents new traction-free boundaries, and induces damage to the rocks near the excavation surface, and thus leads to changes in the hydro-mechanical properties of the near-field rock masses.

As an alternative of the thermodynamics framework, we here illustrate conceptually and phenomenologically how the engineering disturbances affect the coupled processes through the constitutive models. Without losing generality, we introduce a parameter, $\boldsymbol{d}$, to represent the degree of engineering disturbances. The symbol $\boldsymbol{d}$ can be a scalar, a vector or a tensor, which actually reflects the change in rock structures induced by human activities. It can be interpreted as a damage variable or the weakening extent of mechanical properties of rocks by blasting or other excavation techniques, and as a strengthening factor of integrity of the rock mass by bolting and grouting. With this parameter, the constitutive relations in the coupled model can be described as

$$\left.\begin{aligned}&\boldsymbol{D}=\boldsymbol{D}(\boldsymbol{\sigma},\boldsymbol{d})\\&\boldsymbol{k}=\boldsymbol{k}(\boldsymbol{\sigma},\boldsymbol{d})\\&\boldsymbol{\lambda}=\boldsymbol{\lambda}(T,\boldsymbol{\sigma},\boldsymbol{d})\end{aligned}\right\} \tag{9}$$

Equation (9) shows that the disturbance parameter, $\boldsymbol{d}$, changes the rock properties and thus induces

changes in the coupled processes of rocks from their initial equilibrium states. If ***d*** is regarded as a damage variable, the growth of damage induced by blasting will lead to deterioration of elastic moduli, enhancement of permeability, and decrease of thermal conductivity.

Note that in slope engineering, the thermal process may play a secondary role in the coupled system during the engineering lifetime, compared to the effects of mechanical loading/unloading and seepage flow on the stability of slopes in hydropower engineering. Thus, in the remaining sections, the effects of heat transport will not be discussed.

3 Effects of engineering disturbances

3.1 Effects of excavation

The blasting excavation of a rock mass not only leads to quasi-static release of stress by forming new traction-free boundary conditions in the domain of interest, but also results in dynamic unloading effects in the vicinity of the excavation surface under in-situ stresses. Consequently, existing fractures may deform and propagate, and new fractures may be induced, which in turn changes the structure of the near-field rock mass concerned and alters its hydro-mechanical properties.

For deeply cut valley slopes, the geological processes lead to zoning of hydro-mechanical properties of the rock masses away from the bank slope surface. Figure 2 shows a typical section of the valley at the Laxiwa dam site [7].

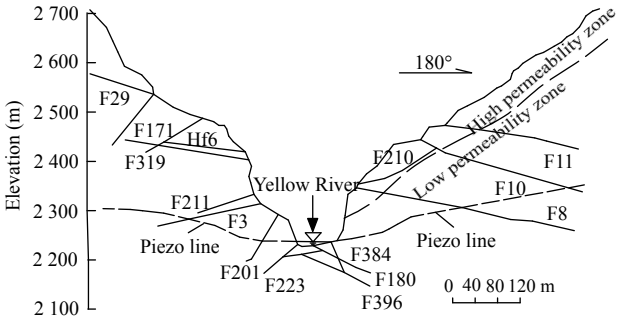

Fig.2 A typical section of the Laxiwa dam site [7].

In-situ investigations [8] showed that stress release-induced fractures were developed in the shallow rock mass on the right bank of the valley. A high permeability zone (k = 10^{-6}–10^{-5} cm/s) of a horizontal overburden of 0–80 m in depth was formed in the bank slope. The stress release-induced fractures, however, became infrequent in the deeper rock mass, and the measured permeability (k = 10^{-7}–10^{-6} cm/s) was generally 1–2 orders of magnitude smaller than the permeability of shallow rock mass. On the other hand, the relatively high permeability zone possessed smaller values of deformation modulus, while larger values were recorded in the low permeability zone.

In the presence of human activities, such as blasting, a disturbed zone will usually be induced, in which considerable weakening of mechanical properties and enhancing of hydraulic properties of the rock masses will be observed. Figure 3 shows the disturbed zone in the permanent shiplock slopes of the Three Gorges project [9]. The permanent shiplock slopes were formed by deeply cutting into weathered and fresh granites, with 1 607 m in length and 50–170 m in height. The disturbed zone was determined by performing comprehensive investigations, including in-situ testing, monitoring, nonlinear finite element modeling, back analysis, and rock mass quality rating [9]. Away from the cut surface, the excavation disturbed zone (EDZ) could be further divided into a damaged zone (DZ), an affected zone (AZ) and a slightly affected zone (SAZ), according to the extent of weakening in the mechanical and physical properties of the rock masses. The damaged and affected zones were 5–10 and 10–20 m in thickness, respectively.

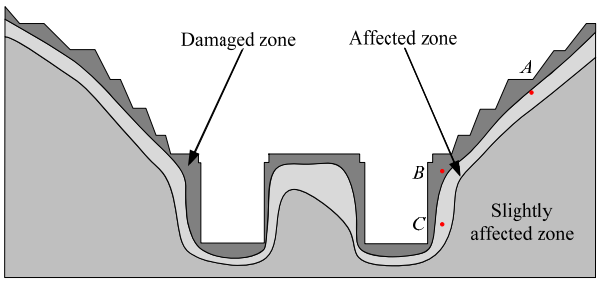

Fig.3 Distribution of disturbed zone in the permanent shiplock slopes [9].

Table 1 summarizes the mean hydro-mechanical properties (acoustic velocity in vertical sidewall, v_a; seismic velocity in monitoring adits, v_{sa}; seismic velocity in separation block, v_{ss}; borehole deformation modulus, E_b; deformation modulus in monitoring adits, E_p; major principal permeability, k) of the rock masses in the three sub-zones by in-situ tests [9, 10]. The major principal permeability was estimated with numerical simulations by considering the geological conditions and the stress states of slope after excavation at three locations (points A–C), 10 m

Table 1 Properties of various zones.

EDZ	v_a (m/s)	v_{sa} (m/s)	v_{ss} (m/s)	E_b (GPa)	E_p (GPa)	k (cm/s)
DZ	3 819	3 210	3 332	22.8	8.0	$(0.71–1.04) \times 10^{-5}$
AZ	4 232	4 470	4 362	27.5	26.6	
SAZ	5 348	4 890	5 247	35.9	48.9	$(4.3–6.5) \times 10^{-7}$

in horizontal depth from the cut surface [10], as shown in Fig.3.

It can be observed from Table 1 that the blasting for the slope excavation resulted in remarkable weakening of deformation modulus and significant enhancement of permeability in the damaged and affected zones. The degrees of weakening of the rock mass deformation modulus measured in the boreholes and tunnels were 37% and 84% in the DZ, and 24% and 46% in the AZ, respectively. The excavation-induced increase in the major principal permeability was estimated up to two orders of magnitude at points *A*–*C*. As a matter of fact, the joint openings in the disturbed zone would lead to a much higher increase in the permeability, even over 3–4 orders of magnitude.

The blasting-induced dynamic unloading may also lead to an opening of existing fractures and enhancement of hydraulic properties [2]. Figure 4 shows a vertically cut slope, in which a family of vertically oriented fractures with a uniform spacing l_i and a zero initial aperture, are developed [2].

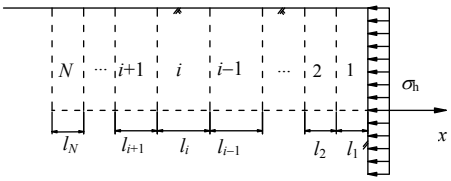

Fig.4 Fracture opening due to an instantaneous release of stress [2].

The fractures cut the rock mass into N blocks. The blasting excavation results in an instantaneous release of horizontal stress σ_h on the cut surface. Neglecting the cohesion of the fractures and elastic rebound of the rock blocks, the openings of the fractures, b, can be estimated by using the principle of conservation of energy. The permeability of the fractured rock mass, k_f, can then be equivalently estimated by applying the well-known cubic law and the averaging concept in the spacing:

$$k_f = \frac{gb^3}{12\nu l} \tag{10}$$

where ν is the kinematic viscosity of water.

For an illustrative study, we take $N = 7$, $l = 5$ m, $\rho = 2\ 700$ kg/m^3 (density of the rock blocks), $\sigma_h = 20$ MPa, $f = 1.0$ (friction coefficient of the fractures), and assume that the moduli of the rock blocks, E, vary from 10 GPa for the first block to 40 GPa for the last one, with a uniform increment of 5 GPa.

Figure 5 gives the distributions of aperture of the fractures and equivalent permeability of the rock mass. It is shown that both aperture and permeability decrease with the increase in horizontal distance away from the cut surface, but the values of the last fracture increase owing to the rigid body displacement of the rock blocks. If the moduli of the rock blocks are assumed to be uniform (40 MPa), no loosing of fractures occurs except for the last fracture.

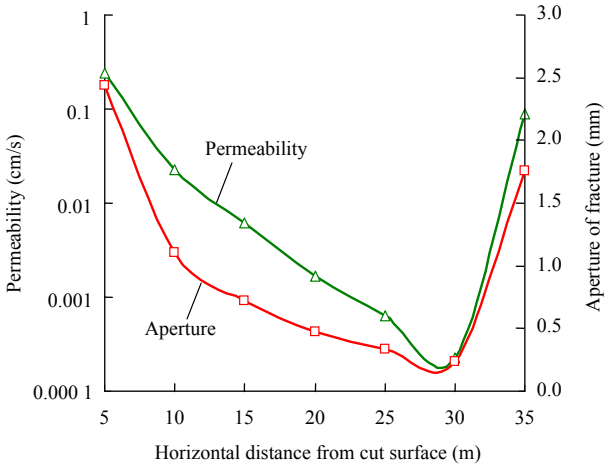

Fig.5 Aperture distribution of fractures and equivalent permeability of rock mass.

3.2 Effects of bolt reinforcement

Bolting is a primary means used to stabilize a natural or excavated slope. It transfers load from unstable exterior to the confined interior of the rock masses. Rock bolts constrain the normal and shear deformations of the fractures in the reinforced rock masses, which increase the applied normal stress on the fractures through prestressing or restrain shear dilatancy, and even change the loading condition of the fractures from constant normal loading to constant stiffness loading conditions [2]. As a result, the bearing capacity of the rock mass is improved and the permeability is changed by the support system.

Figure 6 plots the variations in the permeability of a hard rock fracture with shear displacement under various normal stresses, resultant from shear dilatancy [11]. One can observe from Fig.6 that when the

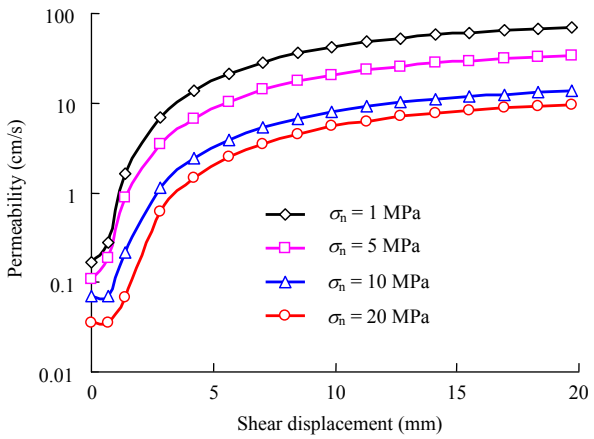

Fig.6 Variations in permeability of a rock fracture with shear displacement [11].

normal stress of the fracture increases or its shear deformation is restrained, as a bolted fracture behaves, the permeability of the fracture will be smaller.

Table 2 lists the principal permeabilities (k_1, k_2 and k_3) of the rock masses after excavation at points *A*–*C* in the permanent shiplock slope of the Three Gorge project (Fig.3) with and without support, respectively [10]. The permeabilities were estimated by numerical simulations in terms of geological conditions and stress states of the slope after excavation. The effect of prestressed bolts was simulated by applying a uniform normal stress on the vertically excavated faces. Calibration studies showed that the predicted results agreed rather well with the reality. Note that the orientations of the principal permeabilities shown in Table 2 with and without support were rather close to each other.

Table 2 Comparison of principal permeabilities of a rock mass with and without support [10].

Point	Support	k_1 (cm/s)	k_2 (cm/s)	k_3 (cm/s)
A	No	0.93×10^{-5}	0.24×10^{-5}	0.13×10^{-5}
	Yes	0.82×10^{-5}	0.23×10^{-5}	0.08×10^{-5}
B	No	1.04×10^{-5}	0.23×10^{-5}	0.08×10^{-5}
	Yes	0.34×10^{-5}	0.13×10^{-5}	0.05×10^{-5}
C	No	0.71×10^{-5}	0.17×10^{-5}	0.06×10^{-5}
	Yes	0.40×10^{-5}	0.11×10^{-5}	0.04×10^{-5}

It can also be observed from Table 2 that the difference in permeability at point *A* with and without support was not manifested since point *A* was rather far away from the retaining system. But the discrepancies at points *B* and *C* were remarkable, especially for the major principal permeability. This indicates that the influence of bolting needs to be considered for estimation of permeability of a reinforced rock mass, especially when the effects of grouts used for rocks are further taken into account (see Section 3.3).

3.3 Effects of grouting

Grouting is commonly used in rock engineering to fill voids and seal fractures with cemented grouting materials in rock masses. Actually, grouting is a process that involves complex thermo-hydro-mechano-chemical (THMC) coupling phenomena during injection, movement and hardening of the grouts, and results in higher integrity and bearing capacity, and lower deformability and permeability of the grouted rock mass.

Before the construction of the Three Gorges dam, grouting was performed for investigating rock mass properties in an exploratory tunnel No.5, oriented along exploratory line III [12]. The tunnel was hosted in weakly weathered granites. The surrounding rocks were separated into test zones *A* and *B*. Cementitious grouting was injected into zone *A* and epoxy resin grouting was injected into zone *B*. Table 3 lists the vertical deformation modulus ($E_{0\perp}$) and elastic modulus ($E_{\perp}$), horizontal deformation modulus ($E_{0//}$) and elastic modulus ($E_{//}$), acoustic velocity (v_a) and permeability (k) of the test zones before and after grouting. It indicates that grouting leads to significant increases in stiffness properties and decreases in permeability of the examined rock mass.

Table 3 Comparison of rock mass properties before and after grouting [12].

Zone	Grouting	$E_{0\perp}$ (GPa)	$E_{\perp}$ (GPa)	$E_{0//}$ (GPa)	$E_{//}$ (GPa)	k (10^{-6} cm/s)	v_a (m/s)
A	Before	0.99	2.11	5.43	9.35	1.27	< 5 000
	After	18.28	21.51	11.00	17.66	0.18	(enhanced for)
B	Before	1.15	2.68	0.18	0.29	0.15–3.75	4 460
	After	1.93	3.08	0.58–2.29	0.92–4.13	0.08–0.91	4 940

4 Influences of seepage on slope deformation and stability

Seepage flow in the soils and rocks of a slope has a great influence on the slope deformation and stability. Recent surveys showed that 95% of landslides in China (including more than 90 case studies) were triggered by groundwater, often in the rainy seasons [10]. Excavation of slope and deployment of drains present new potential seepage boundaries and high permeability zones (in the EDZs) near the cut surfaces

in the field, which may change the flow pattern in the slope and affect its stability state.

Figure 7 shows a homogeneous slope with a constant water supply on the left lateral boundary. The symbols I–IV are the slope excavation steps, and numbers 1–4 are corresponding phreatic lines of slope excavation steps I–IV, respectively.

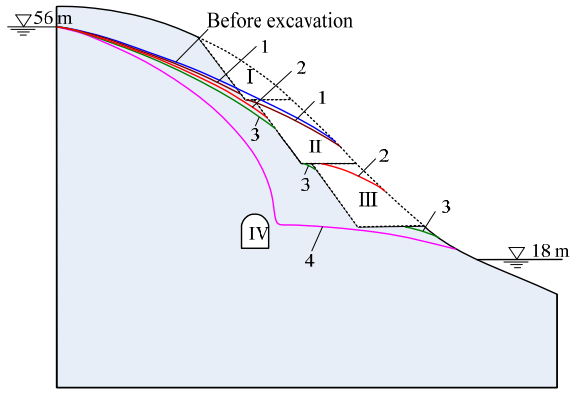

Fig.7 Variations of free surface due to excavation of a slope.

The slope is about 60 m in height and 80 m in width. The left boundary is prescribed with a water head of 56 m, and the right boundary with 18 m. The slope is excavated by three steps and followed by an excavation of a tunnel within the slope. The distributions of the free surface before and after excavation of each step are plotted in Fig.7. It shows that the excavations of the slope significantly decrease the locations of the free surface due to presence of new seepage boundaries on the cut surfaces.

Figure 8 shows another homogeneous slope with horizontal drains [13]. The sizes of the slope are 100 m in maximum height and 150 m in width. Seven rows of horizontal drains are deployed in the slope. The diameter of the drains is 140 mm. Both the vertical and horizontal spacings of the drains are 5 m. The

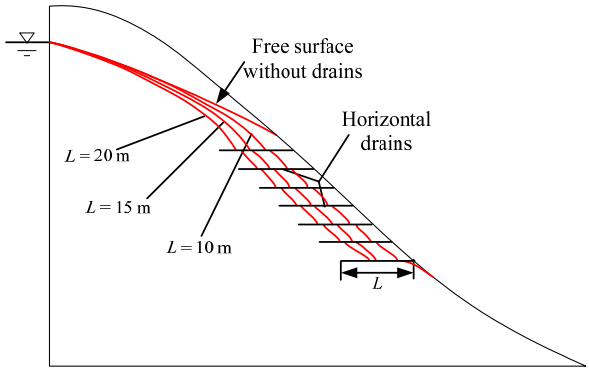

Fig.8 Effect of drains on seepage flow in a slope.

effect of the drain length is investigated by taking the values of 10, 15 and 20 m, respectively. The left boundary is also assumed to have a constant source of water supply, with a prescribed water head of 90 m. The comparison of the locations of the free surfaces with and without drains at different lengths is plotted in Fig.8, which indicates that the drains significantly lower the location of the free surface, especially with the increase in the drain length.

It has been recognized that the lowering of the free surface inside a slope would enhance its stability. To further illustrate how the seepage flow and the drains influence the slope stability, we consider the evolution of stability of an idealized slope induced by rainfall [14]. Figure 9 shows the computational model.

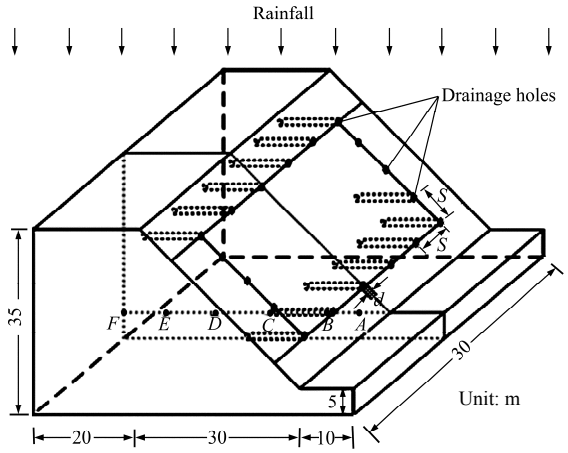

Fig.9 Illustration of an idealized slope under rainfall [14].

The unsaturated soil properties of the slope were given in Ref.[14]. The initial groundwater level is supposed to be horizontal at a lower ground surface. The initial degree of saturation is assumed to be uniform at the slope crest, with S_r = 0.682, and linearly increases to a unity at the height of the initial water level. The rainfall of a constant intensity 30 mm/h is assumed to last for 4 days (96 hours). Horizontal drains of uniform horizontal and vertical spacing are deployed in the slope, with diameter ϕ = 120 mm, length L = 15 m, and spacing S = 5, 10 and 20 m, respectively, for slope stability assessment. Interested readers may refer to Ref.[14] for other properties of the unsaturated soil, including soil-water characteristic curve and shear strength of the soil.

Figure 10 plots the distributions of pressure head at a typical cross-section without drains and with the drains of spacing S = 5 m after 48 hours of rainfall. Figure 10 clearly shows the remarkable effects of the drains on lowering the pore water pressures in the slope. From Fig.10, it can also be observed that there is an unsaturated zone with negative pressure head in

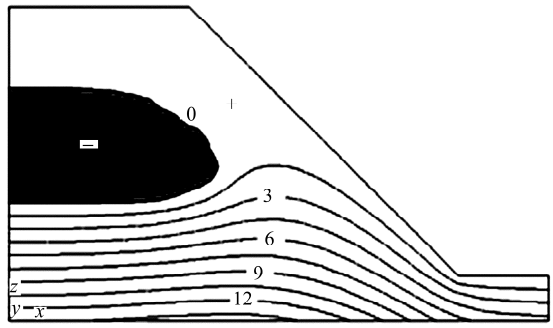

(a) No drains.

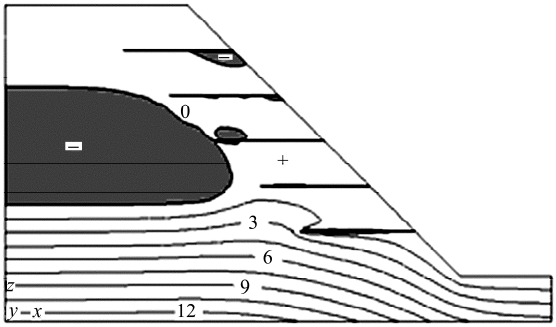

(b) Drains with spacing S = 5 m.

Fig.10 Contours of pressure head after 48 hours of rainfall [14] (unit: m).

the middle of the slope, or in other words, there is a perched water zone with positive pressure head above the unsaturated zone. The unsaturated zone becomes smaller as the infiltration of rainfall proceeds, and disappears abruptly as the connection between the two zones occurs and a steady-state flow behavior is then reached.

Figure 11 shows the evolutions of the factor of safety of the slope for various deployment schemes of the horizontal drains [14], in which the factor of safety is assessed with the Morgenstern-Price method. The factor of safety at the initial state is 1.40, and it evolves to 1.0 after 69.3 hours of rainfall if no drains are installed, meaning that failure of the slope may theoretically occur at that time and the slope reaches a critical state.

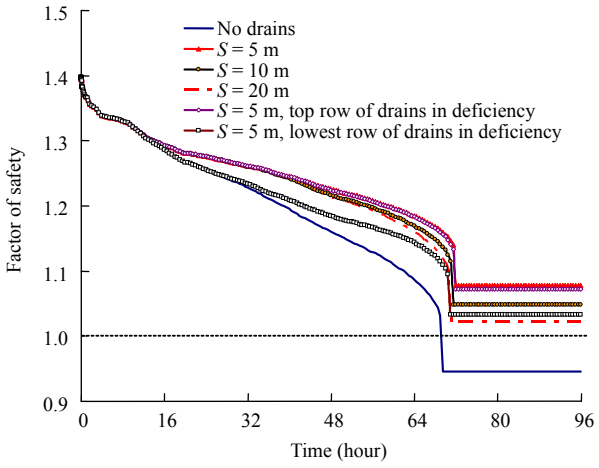

Fig.11 Evolutions of factor of safety for various deployment schemes of horizontal drains [14].

As the whole slope is saturated, the factors of safety are 0.95 and 1.08, for the cases without the horizontal drains and with the drains of S = 5 m, respectively. It can be inferred from the curves that denser spacing of the drains would lead to higher stability of the slope, and as the steady state of infiltration is approached, the factors of safety are increased by 0.13, 0.10 and 0.07 for the cases with the drains of S = 5, 10 and 20 m, respectively, compared to the case without the drains. In addition, for the drains with S = 5 m, the top row has a negligible effect on improving the stability of the slope, but the lowest row has a remarkable one, indicating the importance of the installed locations of the drains in maintaining the stability of the slope.

5 A case study of slope stability analysis and deformation control

5.1 Geological features of the left high slope of Jinping I hydropower station

Jinping I hydropower station is located at the upstream of Yalong River, between Muli and Yanyuan counties in Sichuan Province, China. The double-curvature concrete arch dam of 305 m in height will be the highest concrete arch dam in the world [15]. The dam site is located in a typical deeply cut V-shaped valley, and consequently the geological conditions in the dam site are very complex. The dam left abutment slope is high and steep, as shown in Fig.12.

Fig.12 A deeply cut V-shaped valley at the dam site of Jinping I hydropower station.

The natural slope above the elevation of 1 850 m is mainly composed of sandy slate, with a dip angle varying from 40° to 50°. The natural slope below the elevation of 1 850 m is mainly composed of marble, with a dip angle varying from 55° to 70°. A typical geological profile (II_1-II_1) of the dam site is shown in Fig.13. Faults f_5, f_8 and $f_{42\text{-}9}$, lamprophyre dike (X) and some other weak geological structural features are developed in the dam left abutment slope. Besides, release fractures are widely developed in the subsurface of the slope, even up to 100–200 m in depth. These unfavorable geological structural features lead to poor stability conditions of the slope [16–19]. The dam left abutment slope is of primary importance since its deformation and stability have a direct impact on the construction schedule and even the dam's long-term operation. It serves as a typical case for application of the proposed generalized multi-field coupling approach to deformation and stability control of high slopes.

5.2 Stability and deformation control of the high slope during construction

Stability and deformation control of the dam left abutment slope are key technological issues. Various monitoring measures, including surface and deep deformation surveying, have been taken to explore the stability conditions of the left bank slope [20]. Theodolites and level instruments were installed to record horizontal and vertical displacements on the slope surface, while deep deformation was measured by inclinometer borehole and rod extensometers. Figure 14 shows the monitoring layout at the typical profile II_1-II_1 of the left bank slope.

During construction, slope deformation is mainly caused by excavation-induced unloading, blasting, bolt supporting and rainfalls. The generalized multi-field coupling model can be used to predict the displacements of the slope induced by the coupled effects of stress, seepage and engineering disturbances, and to realize the decoupling of their respective deformation components [21]. Figure 15 shows different deformation components of the surface monitoring point TP5.

It can be observed from Fig.15 that during the period of construction, deformation of the rock masses was mainly caused by excavation-induced unloading, up to about 80% of the total deformation. Blasting played a secondary role in the deformation, and its effect decreased as the blasting surface became far from the measuring point. The deformation component

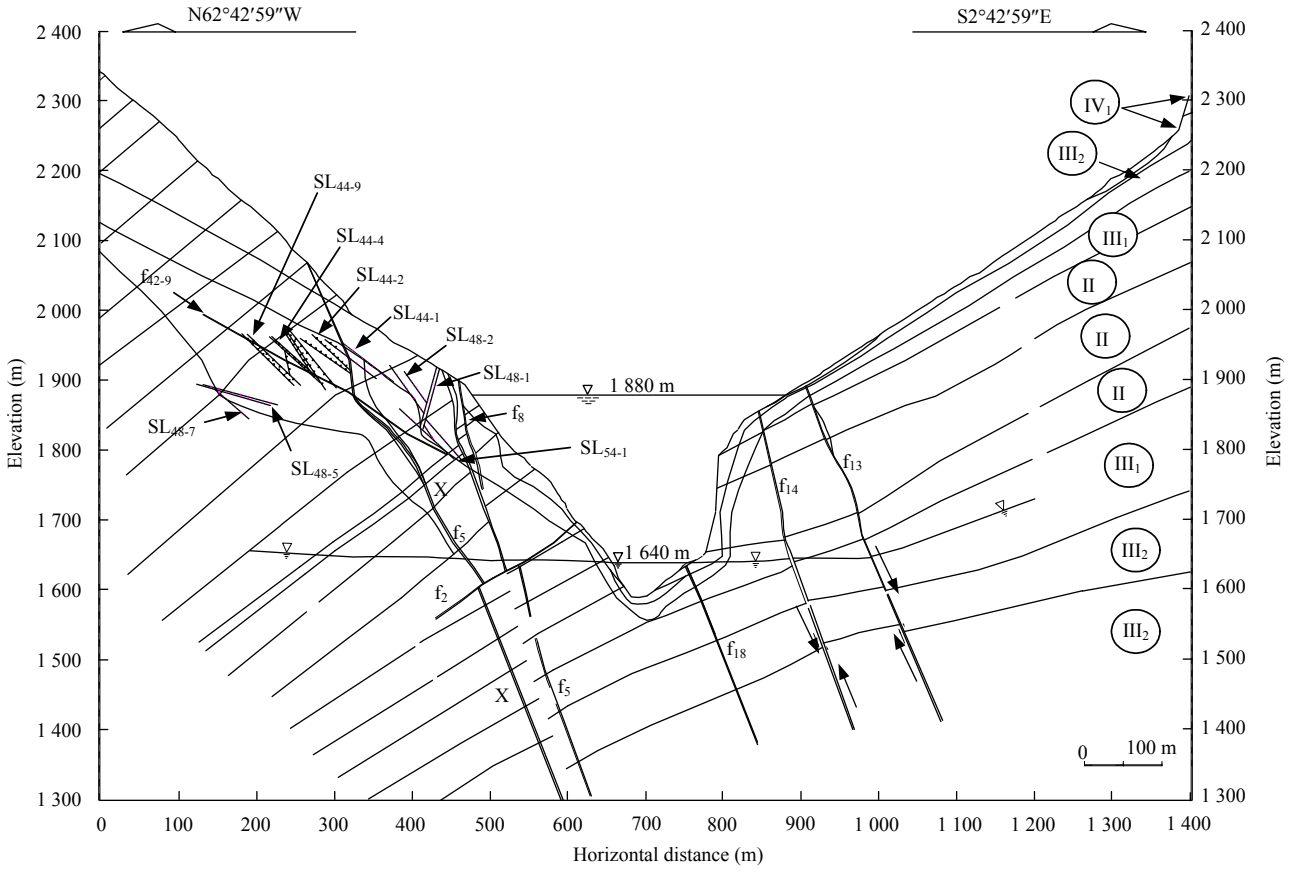

Fig.13 A typical geological profile (II_1-II_1) of the Jinping I hydropower station dam site.

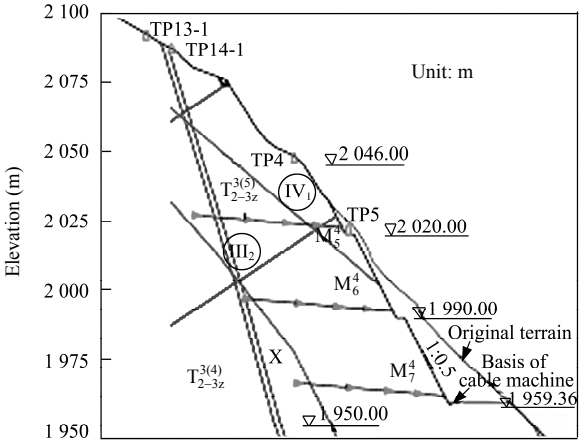

Fig.14 Deformation monitoring layout at a typical slope profile.

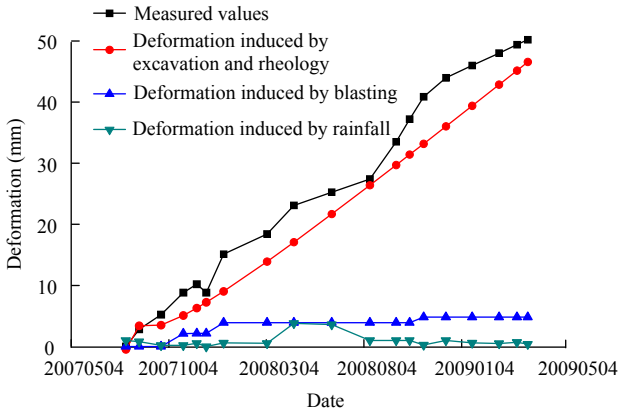

Fig.15 Deformation decoupling of the displacement at TP5.

induced by rainfall was related to the duration and intensity of rainfall. From March to August in 2008, the deformation induced by rainfall was about 15% of the total deformation during rainy season. But after November, 2008, because of an abrupt decrease in rainfall, the deformation induced by rainfall was only about 3% of the total deformation. The results demonstrate that the proposed model can effectively explain the mechanisms of the slope deformation induced by various engineering disturbances and rainfall infiltration.

Considering the effects of blasting and excavation-induced unloading, we simulated the excavation processes of the dam left abutment slope with an elastoplastic model. The shallow rock masses in the slope, i.e. 0–15 m in depth from the slope surface, were defined as the DZ, with the deformation modulus reduced by 67%. The deeper parts of the rock masses, i.e. 15–30 m in depth from the slope surface, were defined as the AZ, with the deformation modulus reduced by 50%. Figure 16 plots the displacement vectors at the II_1-II_1 profile.

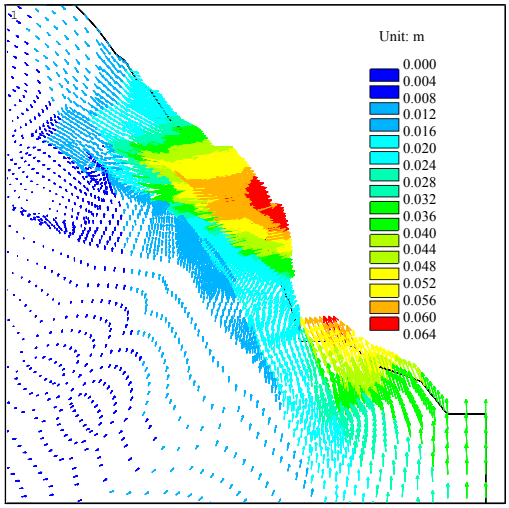

Fig.16 Plot of displacement vectors at the II_1-II_1 profile.

Since the dam left abutment slope is geologically anti-inclined, the rock masses at higher elevations show a trend of toppling failure mode. Affected by the release fractures oriented NE with a dip towards SE, openings of this group of fractures occurred in the EDZ. Affected by a group of small faults parallel to fault $f_{42\text{-}9}$, the deformation in terms of shear slip occurred towards the free face of the slope. Therefore, it can be concluded that unloading-induced deformation by excavation of the dam left abutment slope is mainly controlled by the discontinuities in the rock masses. To improve the stability of the high slope, rock bolts, anchor cables and pre-consolidation grouting were used to reinforce the shallow and surface rock masses of the slope. The reinforcement layout for slope stability and deformation control is shown in Fig.17.

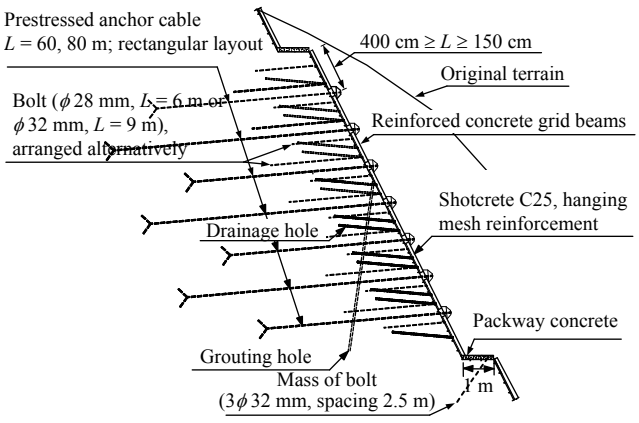

Fig.17 Reinforcement layout for the shallow and surface rock masses.

Determination of the support timing for the

excavated slope is an important issue in controlling the stability of the slope, especially when the slope deformation goes into an accelerative stage. According to the spatial distribution and intersections of the weak structural features in the dam left abutment slope, it can be concluded that the overall stability of the slope is mainly controlled by a tensile dehiscent deformable block formed by fault $f_{42\text{-}9}$, lamprophyre dike (X) and deep fracture $SL_{44\text{-}1}$ (Fig.18). In order to analyze failure mechanism and suitable support timing for the left high slope, some observation points were placed on the positions where the fault $f_{42\text{-}9}$ was exposed on the excavated slope surface (Fig.19).

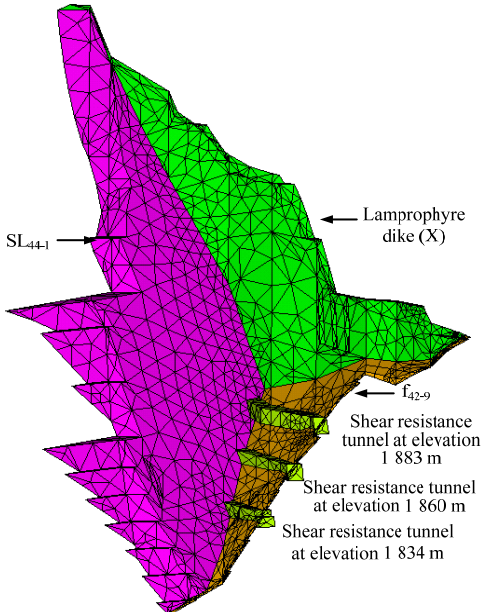

Fig.18 Slip surface boundaries of the huge block and the layout of three shear resistance tunnels.

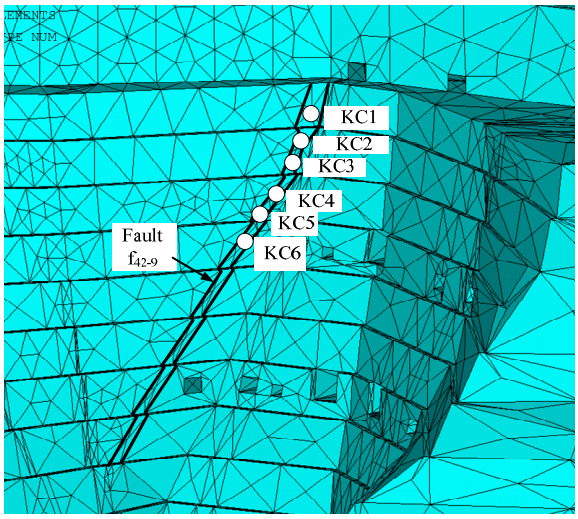

Fig.19 Layout of observation points on the excavated slope surface.

Figure 20 shows the variations of the dislocation deformation at the observation points with the excavation elevations. It is clear that the dislocation deformation in fault $f_{42\text{-}9}$ is caused by the excavation of the cableway platform slope and the spandrel groove slope, but the dislocation deformation mechanisms for these two excavation periods are totally different.

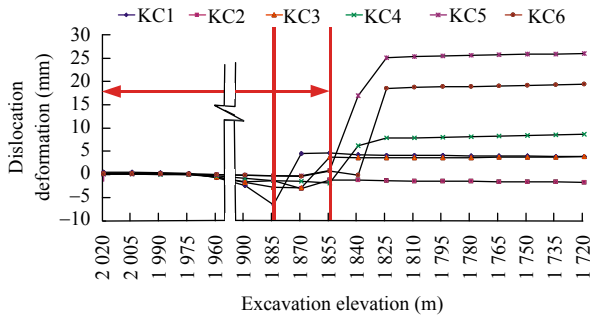

Fig.20 Relationship between the dislocation deformation at the observation points and the excavation elevations.

Unloading rebound dislocation deformation occurred in fault $f_{42\text{-}9}$ during the excavation of the cableway platform slope, whose direction was towards the interior of the slope. However, the direction of the dislocation deformation in fault $f_{42\text{-}9}$ pointed to the free surface of the slope as the rocks, which were removed during the excavation of the spandrel groove slope. This dislocation deformation was significantly increased during the excavation of the slope below elevation 1 855 m, which would drastically deteriorate the stability of the slope. Therefore, the advantageous support timing was that all the three shear resistance tunnels should have been backfilled before the excavation of the slope between elevations 1 855 and 1 825 m. Meanwhile, reinforcement measures for the shallow and surface layers of the rock masses should be taken in order to ensure the stability of the slope during excavation.

The stability of the left high slope after implementation of the reinforcement measures was also evaluated by an interactive visualization tool named Slope^{3D} [22]. For comparison, Table 4 gives the factors of safety of the left bank slope with various reinforcement measures. It is indicated that reinforcement obviously improves the stability of the slope. It can also be seen from Table 4 that the combination of various reinforcement measures, including the shear resistance tunnels, rock bolts and anchor cables, need to be taken to satisfy the design demand (F_s = 1.3).

Table 4 The factors of safety of the left bank slope for various reinforcement measures.

Support	Factor of safety (F_s)		
	Normal operation	Rainfall	Seismic load
None	0.985	0.882	0.845
Shear resistance tunnels	1.204	1.112	1.061
Shear resistance tunnels and anchor cables	1.356	1.255	1.188

By adopting the above integrated engineering measures for slope deformation and stability control, the stability of the dam left abutment slope at Jinping I hydropower station was guaranteed during excavation. The overview of the slope after excavation is shown in Fig.21.

Fig.21 Overview of the left bank slope after excavation.

5.3 Stability and deformation control of the high slope during operation

The engineered slope will be put into operation after the construction of the whole project is completed. From then on, the deformation and stability of the slope will be greatly influenced by its running environments. The hydroelectric engineering slopes are usually subjected to a quite complex running condition, such as impounding of reservoirs, periodical fluctuations of water levels, flood discharge, rainfall and sudden drawdown of reservoir water level, etc. As a result, the seepage of groundwater in the slope and its interactions with other external loads will affect the stability of the slope. Therefore, inappropriate measures in the operation period may cause an increase in slope deformation and a deterioration of slope stability. In the worst case, this will result in failure of the slope globally and other pivot buildings.

The excavation and reinforcement of the dam left abutment slope of Jinping I hydropower station were completed in June, 2009. Based on the field creeping tests of rock masses and the rheological deformation monitoring data, creep back analysis of rocks was performed at the typical section II_1-II_1. The creep parameters of the rock masses, including viscoelastic moduli and the coefficients of viscosity, were obtained. Based on these rheological mechanical parameters, the evolutions of the deformation and stability of the high slope in the left bank in the operation period were predicted with a finite element analysis. During operation, the reservoir water level will fluctuate between 1 800 and 1 880 m. Figure 22 shows the evolution of the displacements perpendicular to the Yalong River at the monitoring points TP5, TPL9, TP13-1 and TPL14 from June, 2009 to June, 2013, considering the seepage effects induced by a sudden drawdown of reservoir water level from 1 880 to 1 800 m.

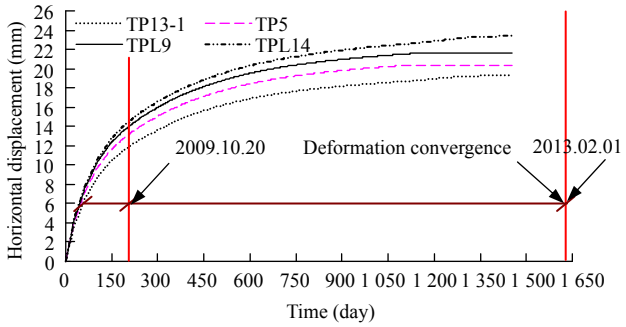

Fig.22 Creep deformation of the left bank slope considering the seepage effect induced by sudden drawdown of reservoir water level.

It can be seen from Fig.23 that the slope displacement perpendicular to the river increases gradually with time, and reaches almost 19.0 mm at higher elevations and up to 20–23.4 mm at lower elevations. The slope rheological deformation tends to be converged after February, 2013, with a displacement velocity less than 0.002 mm per day. In order to examine the effect of multi-field couplings on the slope stability, the creep displacement of the slope produced only by gravity was also simulated and the calculation results are presented in Fig.23. By contrast, it is shown that when the seepage effects are considered, the displacement convergence time of the slope will be delayed by about 3 months and will be increased by more than 7 mm in the extreme condition of a sudden drawdown of the reservoir water level. In addition, the results show that the yielded zone is

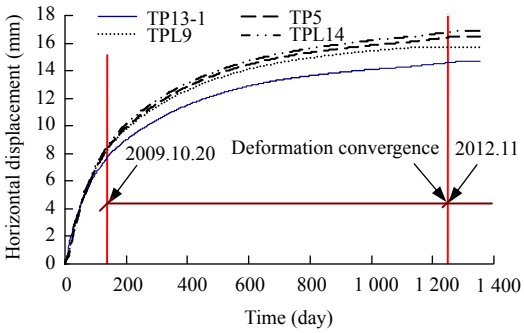

Fig.23 Creep deformation of the left bank slope only induced by gravity

mainly distributed along the fault $f_{42\text{-}9}$ and around the toppling rock masses above the elevation of 1 990 m, after the displacement convergence of the slope, and the size of the zone is much larger than that induced by gravity.

Therefore, the multi-field coupling effects resulting from the environmental changes in the operation period have a significant impact on the deformation and stability evolutions of the slope. Based on the results of performance assessment in the operation period, it is necessary to optimize the layout of the drainage system and to regulate the change rates of the reservoir water level and flood discharge, so as to guarantee the long-term stability during system operation, which is composed of high slopes, a high dam and a huge reservoir.

6 Concluding remarks

Rock masses will be significantly disturbed by human activities, such as blasting excavation, draining, bolting, grouting, etc. These engineering disturbances lead to variations in structural features, boundary conditions and material properties of the rock masses. Consequently, the inherent coupled THM phenomena will be triggered or strengthened in the rock masses, in which the stability state changes. By regarding the engineering disturbances as a controllable man-made process interacting with evolution of the rock masses, a concept of generalized multi-field couplings is proposed in this study.

The generalized multi-field coupling model places particular emphasis on the effects of engineering disturbances on the coupled THM processes by the changes in boundary conditions and rock properties. A parameter, ***d***, which is similar to damage variables but has a broader physical meaning, was conceptually introduced to represent the degree of engineering disturbances and the couplings between the material properties. The effects of blasting excavations, bolt reinforcement, grouting and drainage on the hydro-mechanical properties and stability of slopes in hydropower engineering were systematically estimated with in-situ test data or numerical results.

Research results show that blasting excavation leads to remarkable weakening of deformation modulus and significant enhancing of permeability in the disturbed zone due to both quasi-static and dynamic release of stresses from the cut surfaces. The cementitious or chemical grouting, on the other hand, results in a significant increase in deformation properties and decrease in permeability. Well-known for its enhancement of the bearing capacity and stability of slopes, the bolting is also effective in reducing the rock mass permeability due to the restraints of shear dilatancy of fractures and deformation of the rock masses after applying prestress. The deployment of drains lowers the water tables in slopes or delays the formation of saturated zones during rainfall, hence remarkably enhances the slope stability.

The application of the proposed approach to the deformation and stability control of the dam left abutment at the Jinping I hydropower station further implies the great impacts of blasting excavation, bolt reinforcement, rainfall and reservoir impounding on the slope deformation and stability. Proper excavation schedule, support timing and draining scheme are the key issues to control deformation and maintain stability of the slope during the periods of construction and long-term operation.

It is to be noted, however, that in the proposed generalized multi-field coupling framework, the effects of engineering disturbances on the coupled THM processes should be more comprehensively investigated with field monitoring data and numerical simulations in wider rock engineering practices. The disturbance parameter for description of the degree of engineering disturbances, ***d***, though it seems sound in theory, should be further examined and validated with wider field data for its importance in linking the coupled processes.

Acknowledgements

The authors thank the anonymous reviewers for their valuable comments in improving this study. The data from Chengdu Hydroelectric Investigation and Design Institute of China Hydropower Consulting Group and the relevant literatures are gratefully

acknowledged.

References

[1] Jing L, Tsang C F, Stephansson O. DECOVALEX—an international co-operative research project on mathematical models of coupled THM processes for safety analysis of radioactive waste repositories. International Journal of Rock Mechanics and Mining Sciences, 1995, 32 (5): 389–398.

[2] Zhou C B, Chen Y F, Jiang Q H, Lu W B. Introduction to generalized multi-field coupling analysis for complex rock masses. Beijing: China Water Power Press, 2008 (in Chinese).

[3] Zhou C B, Chen Y F, Jiang Q H, Lu W B. On generalized multi-field coupling for fractured rock masses and its applications to rock engineering. Chinese Journal of Rock Mechanics and Engineering, 2008, 27 (7): 1 329–1 340 (in Chinese).

[4] Rutqvist J, Borgesson L, Chijimatsu M, Kobayashi A, Jing L, Nguyen T S, Noorishad J, Tsang C F. Thermohydromechanics of partially saturated geological media: governing equations and formulation of four finite element models. International Journal of Rock Mechanics and Mining Sciences, 2001, 38 (1): 105–127.

[5] Hudson J A, Stephansson O, Andersson J, Tsang C F, Jing L. Coupled T-H-M issues relating to radioactive waste repository design and performance. International Journal of Rock Mechanics and Mining Sciences, 2001, 38 (1): 143–161.

[6] Chen Y F, Zhou C B, Jing L. Modeling coupled THM processes of geological porous media with multiphase flow: theory and validation against laboratory and field scale experiments. Computers and Geotechnics, 2009, 36 (8): 1 308–1 329.

[7] Zhou C B, Sharma R S, Chen Y F, Rong G. Flow-stress coupled permeability tensor for fractured rock masses. International Journal for Numerical and Analytical Methods in Geomechanics, 2008, 32 (11): 1 289–1 309.

[8] Liu S H. Generation of flow network and field tests on hydraulic conductivity for fractured rock mass. Northwestern Hydropower, 1996, 55 (1): 21–27.

[9] Sheng Q, Yue Z Q, Lee C F, Tham L G, Zhou H. Estimating the excavation disturbed zone in the permanent shiplock slopes of the Three Gorges Project, China. International Journal of Rock Mechanics and Mining Sciences, 2002, 39 (2): 165–184.

[10] Zhang X, Powrie W, Harkness R, Wang S. Estimation of permeability for the rock mass around the shiplocks of the Three Gorges Project, China. International Journal of Rock Mechanics and Mining Sciences, 1999, 36 (3): 381–397.

[11] Chen Y F, Zhou C B, Sheng Y Q. Formulation of strain-dependent hydraulic conductivity for fractured rock mass. International Journal of Rock Mechanics and Mining Sciences, 2007, 44 (7): 981–996.

[12] Ha Q L, Tan R S. Research on grouting of the Three Gorges dam foundation. In: Xiong H J ed. International Development of Anchorage and Grouting in Rocks and Soils. Beijing: China Architecture and Building Press, 1996: 101–113 (in Chinese).

[13] Hu R, Mao X Y, Zhang P. Variational inequality-based seepage flow finite element analysis and its object-oriented programming. Water Resources and Power, 2009, 27 (4): 54–57 (in Chinese).

[14] Chen Y F, Hu R, Zhou C B, Li D Q, Rong G, Jiang Q H. A new classification of seepage control mechanisms in geotechnical engineering. Journal of Rock Mechanics and Geotechnical Engineering, 2010, 2 (3): 209–222.

[15] Institute of Chengdu Investigation and Design of National Electrical Power. Engineering geology report of concretion grout test on relaxed and cracked rock mass at the left slope in the dam site of Jinping I hydropower station. Chengdu: Institute of Chengdu Investigation and Design of National Electrical Power, 2002 (in Chinese).

[16] Gong M F, Qi S W, Liu J. Engineering geological problems related to high geo-stresses at the Jinping I hydropower station, Southwest China. Bulletin of Engineering Geology and the Environment, 2010, 69 (3): 373–380.

[17] Qi S W, Wu F Q, Yan F Z, Lan H X. Mechanism of deep cracks in the left bank slope of Jinping first stage hydropower station. Engineering Geology, 2001, 73(1/2): 129–144.

[18] Rong G, Zhu H C, Wang S J. Primary research on mechanism of deep fractures formation in left bank of Jinping first stage hydropower station. Chinese Journal of Rock Mechanics and Engineering, 2008, 27 (Supp.1): 2 855–2 863 (in Chinese).

[19] Zhou Z, Gong M F, Lei C D. Research on stability of slope at left abutment of Jinping first stage hydropower station. Chinese Journal of Rock Mechanics and Engineering, 2006, 25 (11): 2 298–2 304 (in Chinese).

[20] Zhang J L, Xu W Y, Jin H Y. Safety monitoring and stability analysis of large-scale and complicated high rock slope. Chinese Journal of Rock Mechanics and Engineering, 2009, 28 (9): 1 819–1 827 (in Chinese).

[21] Li C, Jiang Q H, Zhou C B. Forecasting model of slope stability considering deformation mechanism. Rock and Soil Mechanics, 2011, 32 (Supp.1): 545–550 (in Chinese).

[22] Jiang Q H, Wang X H, Feng D X, Feng S R. Slope^{3D} — a three-dimensional limit equilibrium analysis software for slope stability and its application. Chinese Journal of Rock Mechanics and Engineering, 2003, 22 (7): 1 121–1 125 (in Chinese).